

Incommensurate structures studied by a modified Density Matrix Renormalization Group Method

A. Gendiar and A. Šurda

Institute of Physics, Slovak Academy of Sciences, Dúbravská cesta 9,
SK-842 28 Bratislava, Slovak Republic

May 3, 2018

Abstract

A modified density matrix renormalization group *DMRG* method is introduced and applied to classical two-dimensional models: the anisotropic triangular nearest-neighbor Ising (ATNNI) model and the anisotropic triangular next-nearest-neighbor Ising (ANNNI) model. Phase diagrams of both models have complex structures and exhibit incommensurate phases. It was found that the incommensurate phase completely separates the disordered phase from one of the commensurate phases, i. e. the non-existence of the Lifshitz point in phase diagrams of both models was confirmed.

PACS: 05.70.Fh, 64.70.Rh, 02.60.Dc, 02.70.-c

1 Introduction

In 1992 S. R. White [1] invented the density matrix renormalization group (*DMRG*) technique in real space which has been mostly used for diagonalization of one-dimensional (1D) quantum chain spin Hamiltonians. Three years later T. Nishino [2] applied this numerical technique to classical spin 2D models. The *DMRG* method is based on renormalization of the transfer matrix. It is a variational method that maximizes the partition function using a limited number of degrees of freedom and the variational state is written as a product of local matrices [3].

A similar method (cluster transfer matrix method) for classical spin models was developed by one of us, where the variational state is written as a product of local functions [4, 5]. In this paper we shall compare the results of both methods.

The *DMRG* technique proceeds in two steps. In the first one the infinite system method (*ISM*) pushes both ends of the system from each other and enlarges the system by two sites at each iteration. In the second one the finite system method (*FSM*), in which the system has fixed size, improves the values of calculated physical quantities by several left and right moves (sweeps) yielding very accurate results [1].

DMRG has been used for many various quantum models. It provides results with remarkable accuracy for larger systems than it is possible to study using standard diagonalization methods. The 2D classical systems treated by the *DMRG* method exceeds the classical Monte Carlo approach in accuracy, speed, and size of the systems [6]. In spite of this, too few works have been still done for 2D classical spin models by the *DMRG* technique [2, 7, 8]. A further *DMRG* improvement of the classical systems is based on Baxter's corner transfer matrix [9], the *CTMRG* [10], and its generalization to any dimension [11].

The aim of this paper is to investigate two classical models that exhibit incommensurate phases, namely the anisotropic next-nearest-neighbor Ising (ANNNI) model [4] and the anisotropic triangular nearest-neighbor Ising (ATNNI) model [12]. The incommensurate phases were studied by many various theoretical approaches. The free fermion approximation revealed IC phase in 2D classical ANNNI model [13] (also [12] in ATNNI model), 2D incommensurate crystals [14]. Incommensurate structures has been discussed in various topics: 2D C-IC phase transition [15], 2D quantum ANNNI model [16], ANNNI model in $d > 2$ dimensions [17], and by analyzing 1D sine-Gordon model [18] where the authors found no Lifshitz point.

A modified *DMRG* method which can be applicable to more complicated systems, namely the ANNNI and ATNNI models will be developed. Both models are characterized by non-symmetric transfer matrices. The way of how to use *DMRG* in such a case will be described in this paper. Since most work done in *DMRG* has been devoted to the models described by symmetric transfer matrices (2D classical models) or hermitian quantum Hamiltonians (1D quantum models), we show a modified *DMRG* for treating non-symmetric transfer matrix in the ATNNI model. In particular, the existence or non-existence of the Lifshitz point in the ATNNI model will be studied and its phase diagrams will be constructed.

Paper is organized as follows: in Sec. 2 we compare two various methods in using of the *DMRG* technique; in Sec. 3 we describe the ATNNI and ANNNI models; Sec. 4 contains the modified *DMRG* algorithm for the ATNNI model; in Sec. 5 we present our results and in Sec. 6 the results will be summarized and discussed.

2 The DMRG technique for 2D spin systems

For special values of interaction constants both ATNNI and ANNNI models can be reduced to the Ising model. In this case we can compare our approximate *DMRG* calculations with the exact results for infinite 2D models.

Exact results can be relatively easily obtained for 1D models, e.g. strips of finite width. They provide a good opportunity for testing our methods, as well.

The *DMRG* technique as a numerical real-space method, is in fact always applied to finite systems. However, in dependence on the size of the system, it can yield approximate descriptions of 1D or 2D infinite systems.

In case of relatively narrow strips the *DMRG* calculations are consistent with the exact calculations: they yield zero-order parameter and reproduces well the largest and the second largest eigenvalues of the transfer matrix of the system. Comparison of the exact and approximate values for Ising and ATNNI models on a semi-infinite strip of width $L = 16$ with periodic boundary conditions [19] for various approximations are given in Tables 1 and 2. We see that the first two eigenvalues of the superblock transfer matrices in the *DMRG* method are very close to the exact values despite the sizes of superblock matrices ($N \times N$) are much less than the size of the exact T-matrix (65536×65536). The calculations for ATNNI model were performed at a moderate magnetic field $H = 2$. At higher magnetic fields we frequently encountered problems with complex conjugated pairs of two largest transfer matrix eigenvalues in the *DMRG* calculations. Consequent symmetrizing of the density matrix (presented in [20]) did not improved calculations.

A 1D model at non-zero temperature does not display any phase transitions. Nevertheless, the value of the critical temperature for the corresponding 2D model can be found from finite-size scaling (FSS) considerations [21]. This approach represents first of *two methods* we shall use for determination of the critical temperature. Its value for Ising model, derived from

Table 1: *The largest eigenvalues λ_1 and the second largest eigenvalues λ_2 of the transfer matrices calculated with the DMRG technique for the Ising model with periodic boundary conditions. The dimension of the transfer matrix N depends on the size of the block-spin variable [2]. The last line of the table contains the eigenvalues of the transfer matrix obtained by the exact diagonalization method.*

Ising model with periodic boundary conditions				
N	Ordered phase $T = 2.1$		Disordered phase $T = 2.4$	
	λ_1	λ_2	λ_1	λ_2
400	7.00331679 E+06	6.9180364 E+06	1.76379494 E+06	1.5477034 E+06
1600	7.03990343 E+06	6.9742292 E+06	1.76702461 E+06	1.5769844 E+06
3600	7.03991836 E+06	6.9742595 E+06	1.76704324 E+06	1.5771406 E+06
6400	7.04001144 E+06	6.9743133 E+06	1.76710592 E+06	1.5771736 E+06
10000	7.04001146 E+06	6.9743135 E+06	1.76710593 E+06	1.5771740 E+06
65536	7.04001165 E+06	6.9743146 E+06	1.76710598 E+06	1.5771799 E+06

Table 2: *The two largest eigenvalues λ_1 and λ_2 of the transfer matrix for the ATNNI model are calculated with the DMRG technique for periodic boundary conditions [19]. Data obtained by the exact diagonalization method are shown in the last line.*

ATNNI model with periodic boundary conditions				
N	Commensurate phase $T = 0.9, H = 2.0$		Disordered phase $T = 1.2, H = 2.0$	
	λ_1	λ_2	λ_1	λ_2
400	3.8724 E+13	2.4898 E+12	5.8940 E+10	1.0267 E+10
1600	4.0818 E+13	3.7378 E+13	6.9274 E+10	4.5860 E+10
3600	4.0503 E+13	3.7013 E+13	6.9235 E+10	4.5697 E+10
6400	4.0560 E+13	3.7033 E+13	6.9330 E+10	4.5120 E+10
10000	4.0556 E+13	3.6996 E+13	6.9328 E+10	4.4892 E+10
65536	4.0530 E+13	3.6884 E+13	6.9312 E+10	4.4368 E+10

comparing two rescaled semi-infinite strips of width $L = 12$ and 14 with periodic boundary conditions, are the following:

i) $T_c = 2.26987$ from the exact eigenvalues of the transfer matrices of the size $N = 4096$ and $N = 16384$,

ii) $T_c = 2.27008$ from the eigenvalues of the DMRG superblock transfer matrices of the size $N = 1024$

comparing with the exact critical temperature of 2D Ising model $T_c = 2.26918 \dots$ [22].

The second method for determination of the critical temperature is provided by DMRG calculations on 2D systems, large in both directions. Here, below the critical temperature a spontaneous symmetry breaking occurs, i.e. the order parameter acquires non-zero values and tends to zero at the critical point. The DMRG method behaves in a mean-field-like manner. As now T_c can be determined directly, no finite size scaling is necessary. Its accuracy improves with the size of the superblock transfer matrix as follows:

i) $T_c = 2.275$ for $N = 1024$,

- ii) $T_c = 2.272$ for $N = 3600$,
- iii) $T_c = 2.2692$ for $N = 19600$.

For lower orders of approximation the accuracy of this method is worse than of the first one, but it converges faster to the exact value. For the ATNNI and ANNNI models in the phases with broken symmetry, the method explicitly gives the structure of commensurate as well as incommensurate phase. In contrast to the FSS method, it is applicable also in the high magnetic field region and we were able to investigate nearly the whole phase diagram of the model.

3 ATNNI and ANNNI models

(I) The ATNNI model

We consider the two-dimensional classical Ising model with antiferromagnetic interactions between nearest neighbors on a triangular lattice (the ATNNI model). Its Hamiltonian is as follows:

$$\mathcal{H} = \sum_i J \left(\sum_{\hat{\delta}=\hat{1},\hat{2}} \sigma_i \sigma_{i+\hat{\delta}} + \alpha \sigma_i \sigma_{i+\hat{3}} \right) - H \sum_i \sigma_i \quad (1)$$

with $J > 0$, $0 < \alpha < 1$, and the directions $\hat{1}$, $\hat{2}$, $\hat{3}$ where $\sigma_i = \pm 1$, as depicted in Figure 1 (a).

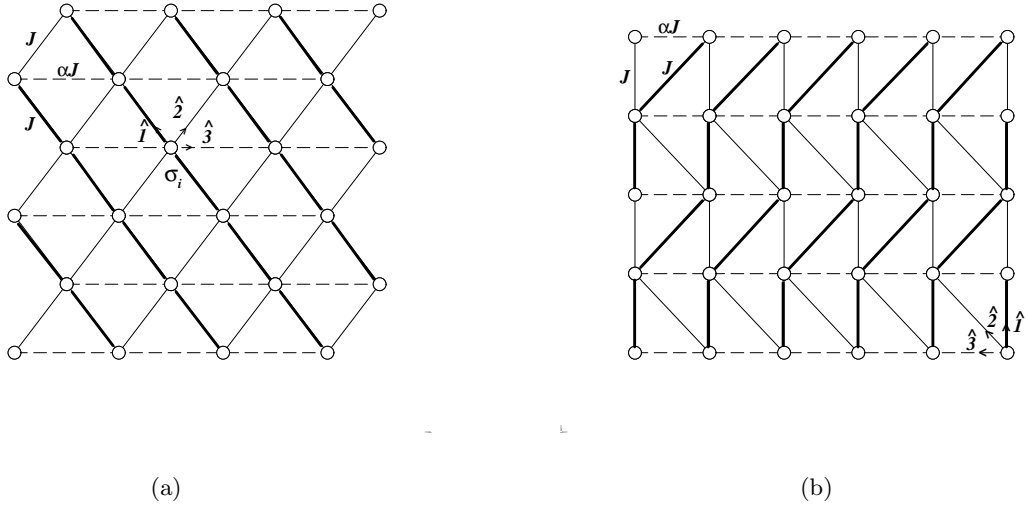


Figure 1: (a) *Triangular lattice of the ATNNI model. Along $\hat{3}$ direction (dashed lines) the incommensurate structure appears;* (b) *The same lattice model designed to transfer matrices that are located here as the horizontal strips. Now the direction $\hat{1}$ in Figure (a) corresponds to thick lines in Figure (b).*

The partition function $\mathcal{Z} = \sum_{\{\sigma\}} e^{-\beta\mathcal{H}}$ where $\beta = (k_B T)^{-1}$ can be written as a product of two types of Boltzmann weights. Each Boltzmann weight $W_B(\sigma_1 \sigma_2 | \sigma'_1 \sigma'_2)$ is composed of four spins which interact among themselves as seen in Figure 2.

The model is exactly solvable for the external magnetic field $H = 0$. At nonzero temperature ($T_c \approx 1.55$ for $\alpha = 0.4$ [12]), it exhibits the second order phase transition. Throughout

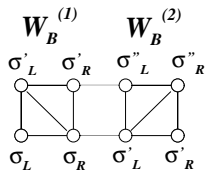


Figure 2: *Two different Boltzmann weights that differ from each other by the orientation of diagonal interactions.*

this paper all numerical calculations are performed at the fixed constant $\alpha = 0.4$, normalization $J = 1$, the dimensionless temperature T/J , and dimensionless ratio H/T in order to compare our results with those obtained in [12].

The numerical calculations are based on a diagonalization of two transfer matrices (in next Sec. we offer more detailed description of their construction). For this purpose we used a square lattice depicted in Figure 1(b) which is related to the initial triangular lattice of the ATNNI model as seen in Figure 1(a). We identify direction $\hat{3}$ with the interaction αJ (Figure 1). In this direction the incommensurate modulation should appear. We use the row-to-row transfer matrices [12].

(II) The ANNNI model

The ANNNI model is defined on the 2D triangular lattice with nearest-neighbor ferromagnetic interactions $J_1 < 0$ for all three directions and a next-nearest-neighbor antiferromagnetic interaction $J_2 > 0$ in one of three directions only. Its Hamiltonian can be written as

$$\mathcal{H} = \sum_i \left(\sum_{\hat{\delta}=\hat{1},\hat{2},\hat{3}} J_1 \sigma_i \sigma_{i+\hat{\delta}} + J_2 \sigma_i \sigma_{i+\hat{4}} \right). \quad (2)$$

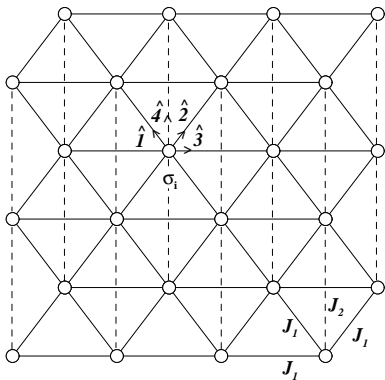


Figure 3: *The 2D ANNNI model on the triangular lattice. Directions $\hat{1}$, $\hat{2}$, and $\hat{3}$ characterize the ferromagnetic interaction J_1 . The next-nearest-neighbor antiferromagnetic interaction J_2 (dashed line) acts in the direction $\hat{4}$ in which the incommensurate phase appears.*

The ANNNI model is usually defined on the square lattice where the next-nearest-neighbor interactions, in fact, are equal to zero and the third-nearest-neighbor ones are non-zero and

antiferromagnetic. The ANNNI model on the triangular lattice is the real Anisotropic Next-Nearest-Neighbor Interaction model with non-zero next-nearest-neighbor interactions and vanishing the third-nearest-neighbor ones. A frustration of the ANNNI model appears due to the competing interactions. The ANNNI model was mostly studied on the square lattice [23] but it was shown by [4] that the properties of the ANNNI model on the triangular lattices remain essentially unchanged.

Boltzmann weight is composed of six spins $W_B(\sigma_1\sigma_2\sigma_3|\sigma'_1\sigma'_2\sigma'_3)$.

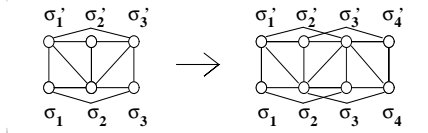


Figure 4: *The six-spin Boltzmann weights of the ANNNI model differing from each other by the orientation of diagonal interactions. In the DMRG calculation the Boltzmann weight defined on the eight-spin cluster was used. It is composed of two overlapping six-spin Boltzmann weights.*

The phase diagram of the ANNNI model (will be discussed in Sec. 5) consists of four regions: ferromagnetic phase with non-zero total magnetization, commensurate phase $\langle 2 \rangle$ with periodically alternating spin signs $(\dots ++ -- ++ \dots)$, paramagnetic phase, and incommensurate phase located between the commensurate and paramagnetic phases.

4 Modification of the DMRG algorithm

The *DMRG* algorithm for quantum models introduced by White [1] was modified and applied for 2D classical lattice models by Nishino [2]. As the ATNNI and ANNNI model on the triangular lattice lead to non-symmetric transfer matrices and incommensurate phases, the Nishino's approach has to be modified further. We shall pursue the second approach discussed in Section 2 – the *DMRG* method applied to very wide strips where the spontaneous symmetry breaking occurs.

The *DMRG* method replaces the exact row-to-row transfer matrix of a strip, which is a product of plaquette Boltzmann weights, by a set of much smaller superblock transfer matrices for every plaquette. The superblock transfer matrix consists of the Boltzmann weight iW_B of the plaquette i multiplied by left and right transfer matrices (blocks) iT_L , iT_R which replace all the remaining plaquette Boltzmann weights of the exact transfer matrix to the left and right from the plaquette. The left and right transfer matrices are indexed by left and right spins $\sigma_{L,R} = \pm 1$ of the plaquette, respectively, and by block-spin variables $\xi = 1, \dots, m$. The number of spin components m determines the order of the approximation. For a modulated phase, iT_L and iT_R differ for each plaquette and, in the *FSM*, are calculated self-consistently from the transfer matrices corresponding to neighboring plaquettes. The left block ${}^{i+1}T_L$ is obtained from ${}^iT_L {}^iW_B$ after a reduction of its matrix size to the original value in a proper way. The right block ${}^{i-1}T_R$ is similarly calculated from ${}^iW_B {}^iT_R$. A calculation of the left and right transfer matrices is performed iteratively during a number of sweeps across the strip.

The reduction of the size of the transfer matrices is based on density matrices that are constructed from the left and right (or in Figure 1(b) and 5 rather upper and lower) eigenvectors of the superblock matrix [1].

The above-described procedure for homogeneous phases and symmetric transfer matrices

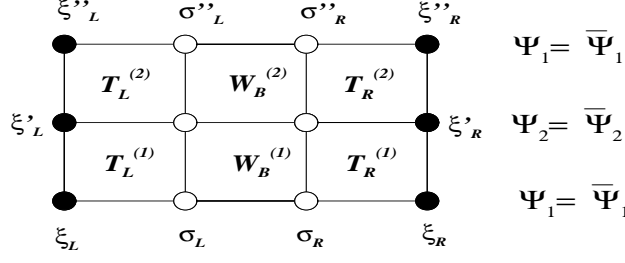


Figure 5: $\Psi_1, \bar{\Psi}_1$ are the right and left eigenvectors that correspond to the largest eigenvalue of the superblock transfer matrices $iT^{(1)} = iT_L^{(1)}iW_B^{(1)}iT_R^{(1)}$ and $iT^{(2)} = iT_L^{(2)}iW_B^{(2)}iT_R^{(2)}$, respectively. Vectors Ψ_2 and $\bar{\Psi}_2$ are needed to calculate a density matrix in each DMRG iteration.

is thoroughly explained in [2]. For the ATNNI and ANNNI models the method should be slightly modified because the transfer matrices are not symmetric and the structure is modulated in both direction, in one of them, incommensurately. It is convenient to choose the strip perpendicularly to the direction of the incommensurate modulation with commensurate structure along the strip, i.e. the strip is orientated in the vertical direction of the lattice shown in Figure 1b. It is seen that there are two different row-to-row non-symmetric transfer matrices in the strip. One transfer matrix is constructed from the Boltzmann weight $W_B^{(1)}$ and the other one from the $W_B^{(2)}$ (Figure 1(b) and 5).

The number of superblock transfer matrices should be equal to at least two, as number of the Boltzmann weights they are attached to. For DMRG with spontaneous symmetry breaking and spatially modulated structures, they may be different for each plaquette of the lattice. The density matrices are not constructed from the eigenvectors of the superblock transfer matrices but rather from functions obtained by an iterative procedure $\Psi_j = \prod_{k=1}^j T^{(k)}\Psi_1$ starting from Ψ_1 given by suitable boundary conditions. For a homogeneous structure and large j the function Ψ_j is identical to the eigenvector of the superblock T .

Fortunately, all the commensurate structures of ATNNI model are as a maximum of period 2 in the direction of the strip. Then, we have only two superblock transfer matrices $T^{(1)} = T_L^{(1)}W_B^{(1)}T_R^{(1)}$ and $T^{(2)} = T_L^{(2)}W_B^{(2)}T_R^{(2)}$ shown in Fig. 5, however, they are dependent on the position of the plaquette in the horizontal (perpendicular to the strip) direction. Similarly, as a result of the iteration procedure we obtain only two different functions Ψ_j where Ψ_1 is the eigenvector of the matrix $T^{(2)}T^{(1)}$ for j even and Ψ_2 is the eigenvector of the matrix product $T^{(1)}T^{(2)}$ for j odd. These both combined matrices are already symmetric and their right and left eigenvectors, Ψ and $\bar{\Psi}$, respectively, are identical.

Writing down the spin variables explicitly, the right eigenvectors are given by the equation

$$\sum_{\xi_L \sigma_L \sigma_R \xi_R} T(\xi_L'' \sigma_L'' \sigma_R'' \xi_R'' | \xi_L \sigma_L \sigma_R \xi_R) \Psi_1(\xi_L \sigma_L \sigma_R \xi_R) = \lambda \Psi_1(\xi_L'' \sigma_L'' \sigma_R'' \xi_R'') \quad (3)$$

where

$$T(\xi_L'' \sigma_L'' \sigma_R'' \xi_R'' | \xi_L \sigma_L \sigma_R \xi_R) = \sum_{\xi_L' \sigma_L' \sigma_R' \xi_R'} T^{(2)}(\xi_L'' \sigma_L'' \sigma_R'' \xi_R'' | \xi_L' \sigma_L' \sigma_R' \xi_R') T^{(1)}(\xi_L' \sigma_L' \sigma_R' \xi_R' | \xi_L \sigma_L \sigma_R \xi_R). \quad (4)$$

The eigenvectors at the odd rows Ψ_2 follow directly from Ψ_1

$$\Psi_2 = T^{(1)}\Psi_1. \quad (5)$$

Optimum size reduction of the matrix ${}^i T_L {}^i W_B$ is performed by its multiplying at both sides by rectangular matrices consisting of several eigenvectors of a density matrix that corresponds to its largest eigenvalues [1, 2]. The density matrix at a row j is constructed from the left and right eigenvectors $\Psi_j, \bar{\Psi}_j$ [5] of transfer matrices with their left and right spins, respectively, lying on the row. For modulated commensurate structures of a period p , the successive functions Ψ_j are not the eigenvectors of one transfer matrix but of a product of p transfer matrices. As for ATNNI model we have two different kinds of rows and different left and right transfer matrices in superblocks, we need four different density matrices. The left density matrices have the following forms:

$$\rho_L^{(1)}(\xi_L^a \sigma_L^a | \xi_L^b \sigma_L^b) = \sum_{\sigma_R^c \xi_R^c} \Psi_1(\xi_L^a \sigma_L^a \sigma_R^c \xi_R^c) \bar{\Psi}_1(\xi_L^b \sigma_L^b \sigma_R^c \xi_R^c) \quad (6)$$

$$\rho_L^{(2)}(\xi_L^{'a} \sigma_L^{'a} | \xi_L^{'b} \sigma_L^{'b}) = \sum_{\sigma_R^{'c} \xi_R^{'c}} \Psi_2(\xi_L^{'a} \sigma_L^{'a} \sigma_R^{'c} \xi_R^{'c}) \bar{\Psi}_2(\xi_L^{'b} \sigma_L^{'b} \sigma_R^{'c} \xi_R^{'c}) \quad (7)$$

In the expressions for the right ones, the summation is performed over the left spins. The functions Ψ_j and $\bar{\Psi}_j$ are identical that is why the density matrices in Eqns.6 and 7 are symmetric. Here we should emphasize that the right blocks T_R are not mirror reflections of the left blocks T_L as they were in the standard approach [1].

By diagonalization of the left symmetric density matrix one obtains a matrix of orthonormal eigenvectors O_L :

$$Q_L(k | \xi \sigma) \rho_L^{(1)}(\xi \sigma | \xi' \sigma') O_L(\xi' \sigma' | \ell) = \omega_k \delta_{k\ell} \quad (8)$$

where Q_L is transposed O_L and the eigenvalues ω_k satisfies the relation

$$\sum_k \omega_k = 1. \quad (9)$$

Analogously, we repeat this procedure for the density matrix $\rho_L^{(2)}$ and $\rho_R^{(2)}$ in order to obtain matrices $Q'_L, O'_L, Q'_R,$ and O'_R . Discarding half eigenvectors in the matrices Q and O that correspond to the smallest eigenvalues ω_k , the matrices O and Q can be used as the reduction matrices in calculation of ${}^{i+1} T_L^{(1)new}$ via

$${}^{i+1} T_L^{(1)new}(\xi_L^{'new} \sigma_L^{'new} | \xi_L^{new} \sigma_L^{new}) = \sum_{\xi_L \xi_L' \sigma_L \sigma_L'} {}^i Q'_L(\xi_L^{'new} | \xi_L' \sigma_L') {}^i T_L^{(1)}(\xi_L' \sigma_L' | \xi_L \sigma_L) {}^i W_B^{(1)}(\sigma_L' \sigma_L^{'new} | \sigma_L \sigma_L^{new}) {}^i O_L(\xi_L \sigma_L | \xi_L^{new}) \quad (10)$$

Generalization for the right block is straightforward. The graphical representation of Eqn. 10 is in Figure 6.

Notice that at this step (Figure 6) the reduction matrix O_L is obtained from diagonalization of the density matrix $\rho_L^{(1)}$ whereas the matrix Q'_L is taken from the diagonalization of the density matrix $\rho_L^{(2)}$. From the knowledge of the functions $\Psi_1, \Psi_2, \bar{\Psi}_1,$ and $\bar{\Psi}_2$ various physical quantities can be found, e.g. site magnetization used in further calculations

$$\langle \sigma_L \rangle = \sum_{\xi_L \sigma_L \sigma_R \xi_R} \Psi_1(\xi_L \sigma_L \sigma_R \xi_R) \sigma_L \bar{\Psi}_1(\xi_L \sigma_L \sigma_R \xi_R). \quad (11)$$

For the ANNNI model, containing also next-nearest-neighbor interactions, the *DMRG* method should be modified further. The left and right block transfer matrices should be indexed, besides the block-spin variable ξ , by four spins σ . The Boltzmann weight is defined

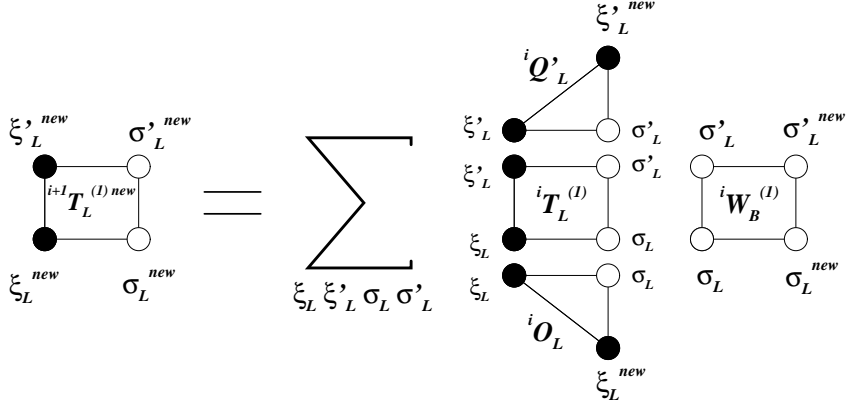


Figure 6: Schematically written equation (10) which we use for computing of the new left renormalized transfer matrix $T_L^{(1) new}$ from the old one $T_L^{(1)}$.

on a plaquette of at least six spins. We have constructed the superblock transfer matrix T from the two block transfer matrices and the Boltzmann weight on an eight-site plaquette (Figure 4) as follows

$$T(\xi_L \sigma_1 \sigma_2 \sigma_3 \sigma_4 \xi_R | \xi'_L \sigma'_1 \sigma'_2 \sigma'_3 \sigma'_4 \xi'_R) = T_L(\xi_L \sigma_1 \sigma_2 | \xi'_L \sigma'_1 \sigma'_2) W_B^{(1)}(\sigma_1 \sigma_2 \sigma_3 | \sigma'_1 \sigma'_2 \sigma'_3) \times W_B^{(2)}(\sigma_2 \sigma_3 \sigma_4 | \sigma'_2 \sigma'_3 \sigma'_4) T_R(\sigma_3 \sigma_4 \xi_R | \sigma'_3 \sigma'_4 \xi'_R) \quad (12)$$

5 Results

The properties of the ANNNI model on the triangular lattice were calculated recently [4] by the cluster transfer matrix method [24]. The results were consistent with numerous calculations of the ANNNI model on the square lattice. To compare performance of the *DMRG* method for incommensurate (IC) structures with other methods we calculated the phase diagram of the ANNNI model shown in Figure 7(a). The resulting diagram is in accordance with previous calculations (Figure 7(b)). We have confirmed general opinion that there is no Lifshitz point on the ferro-para phase transition line.

The region of the IC structure comes out from the *DMRG* rather wide, however, we have used a low-order approximation ($N = 400$). For higher-order approximations the IC-phase region becomes narrower.

The phase diagram of the ATNNI model (in Figure 8) consists of four regions (two different commensurate phases, incommensurate and disordered phase). Characteristic spin structure of both commensurate $\langle I \rangle$ and $\langle II \rangle$ phases of the triangular lattice (Figure 1(a)) is shown in the insets of the same phase diagram.

The phases $\langle I \rangle$ and $\langle II \rangle$ consists of two and three different sublattices with constant magnetization, respectively. In the IC phase, the magnetization of each sublattice is periodically modulated and the sublattices become equivalent to each other. That is why we only plot magnetization of one of these sublattices in some of the following Figures 9 and 10.

The phase diagram was derived from calculation of magnetization. The *DMRG* method with spontaneous symmetry breaking yields directly the space modulation of the magnetization which enables to identify the phase unambiguously. In practical calculations, it is even enough to observe the behavior of the largest eigenvalues of the superblock matrix. The period of their spatial modulation is the same as the period of the structure.

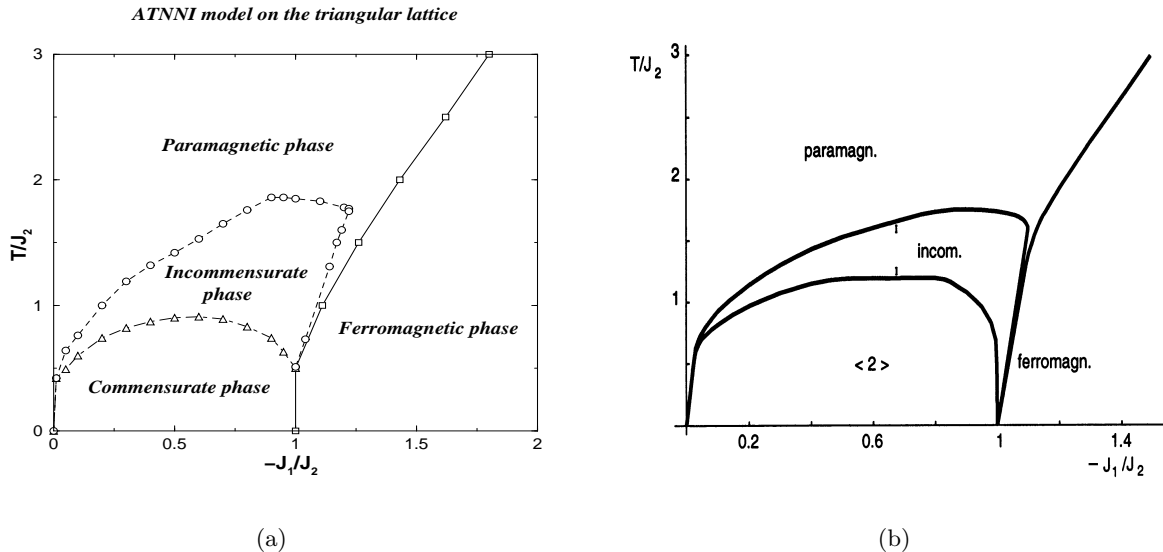


Figure 7: (a) The phase diagram of the ANNNI model obtained by the DMRG method for relatively small superblock transfer-matrix size of $N = 400$. After increasing the superblock transfer-matrix size, the IC region becomes narrower and the para-IC phase transition line is shifted to lower temperatures. (b) The phase diagram constructed with the cluster transfer matrix method [4].

The incommensurate structure is floating, i.e. it is not fixed to the underlying lattice. In our calculation with spontaneous symmetry breaking, one of the infinitely many positions of the incommensurate wave is chosen at the beginning of the calculation and then it remains fixed during the whole further calculation.

We have found the incommensurate structure practically along the whole border between the commensurate $\langle II \rangle$ phase and the disordered phase. However, in two regions the calculations were inconclusive. The high degeneracy of the ground state at $H = 2.4$ and $T < 0.4$ [12] has also caused highly degenerate largest eigenvalues of the superblock transfer matrix, and our method did not converge to any periodic structure for magnetic fields between 2.40 and 2.41 at low temperatures.

The other region, where difficulties were encountered, is located at the high-magnetic-field end ($H = 4.8$) of the phase diagram. Here, the incommensurate phase is extremely narrow (Figure 9(a)) and it has a very large period (Figure 10(b)). Moreover, due to the proximity of the second-order phase transition line, the convergence is very slow.

We have started the calculation with the *ISM* where the superblock transfer matrix is constructed from left and right transfer matrices of the *previous iteration step*. After a large enough number of iterations we obtained a final result for commensurate structures including the disordered phase. For the incommensurate structure it is necessary to perform afterwards some sweeps of the *FSM*, where for the left sweep, the left transfer matrices are taken from the *previous sweep* (analogously, for the right sweep).

The IC structure appears already after the application of the *ISM* but the correct shape of the magnetization is acquired after the *FSM*, only.

The shape of period of the IC structure changes with magnetic field H and temperature T . The period of the IC structure increases with the increasing magnetic field and decreasing

ATNNI model on the triangular lattice

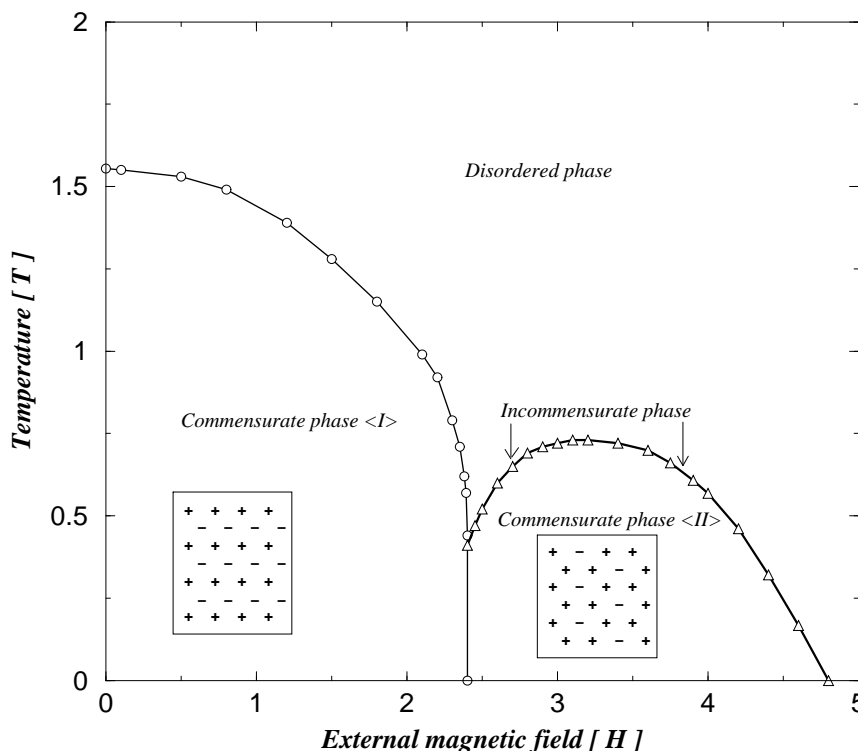


Figure 8: *The entire phase diagram of the ATNNI model is constructed by the DMRG technique. The incommensurate phase appears in narrow region located between the disordered phase and the commensurate phase $\langle II \rangle$ for $2.4 < H < 4.8$. The ATNNI model is highly degenerated for $H = 2.4$.*

temperature. At low temperatures (close to $\langle II \rangle$ –IC phase transition line) the structure consists of wide domains of the phase $\langle II \rangle$ separated by narrow domain walls. At higher temperatures near to disorder–IC transition, the domain walls become wider, the period shorter and the structure acquires a sinusoidal-like shape.

Both phase transitions are continuous. Inverse period of the structure and wave amplitude tend to zero at the $\langle II \rangle$ –IC and disorder–IC phase transition lines, respectively. It should be noted that the notions of low and high temperatures must be understood within an extremely narrow temperature interval where the IC phase exists.

The effect of magnetic field on the IC phase is similar (but inverse) to the temperature effects. Low magnetic field (near 2.4) enhances the high temperature effects, while the high magnetic field (near 4.8) the low temperature ones.

For the magnetic field H close to the value of 4.8, the period is very long, that is why we were able to perform the *ISM* only with an incorrect magnetization shape which would need a further improvement with the *FSM* (Figure 10(b)).

Our calculations converged to the stable periodic solution at the most part of the commensurate $\langle II \rangle$ –disordered phase borders. Here, the IC phase has been found everywhere. This fact leads us to a conjecture (in contrary to [12]) that the Lifshitz point does not exist in the ATNNI model.

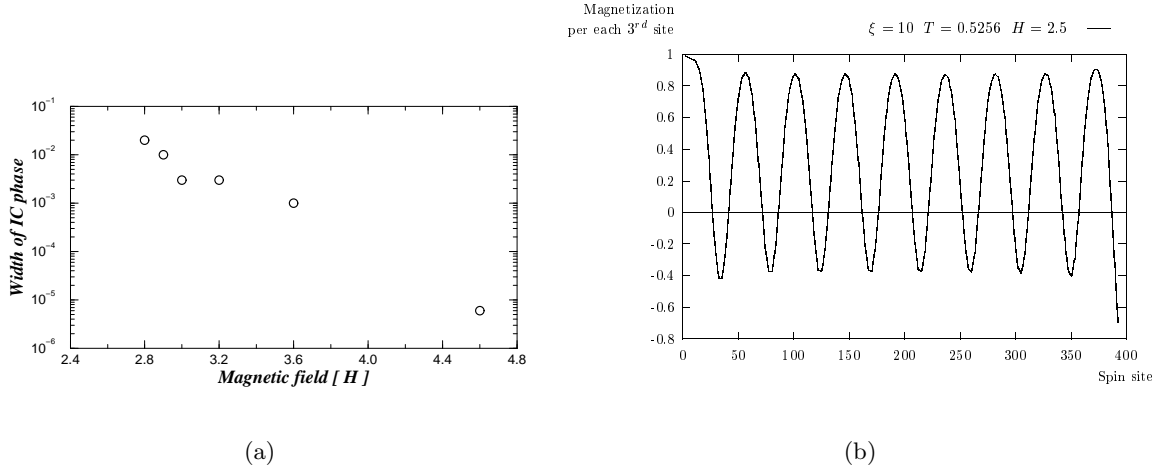


Figure 9: (a) The width of the incommensurate phase measured in units of temperature vs. external magnetic field H . As the field H is increased the distance between the disordered and commensurate phases $\langle II \rangle$ becomes shorter; (b) Measured magnetization per each third spin site using Eqn. (11) inside the incommensurate phase as a function of the spin position on the lattice for $H = 2.5$ and $T = 0.5256$.

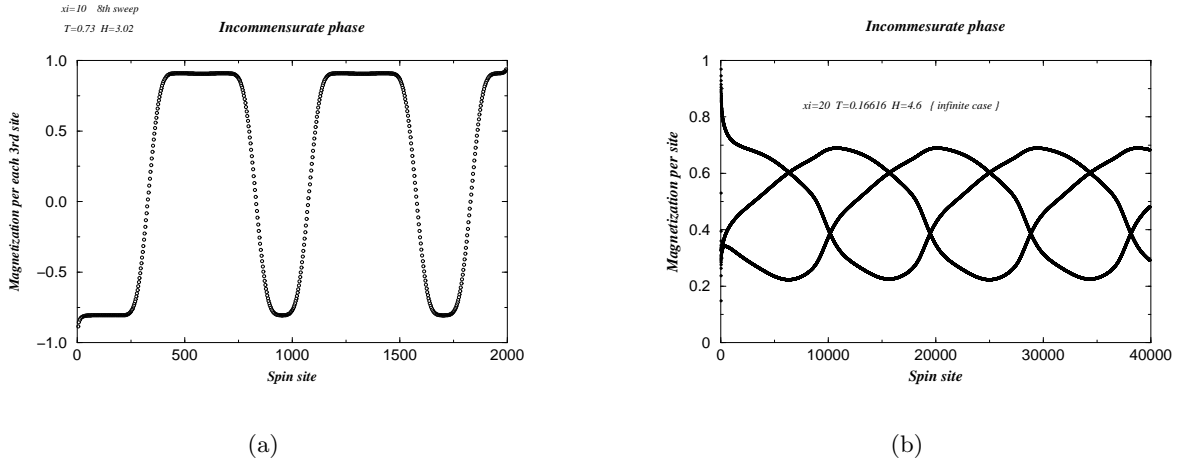


Figure 10: (a) Magnetization vs. position on the lattice measured inside the IC phase on each third site for $H = 3.02$ and $T = 0.73$; (b) IC phase obtained for the large magnetic field $H = 4.6$ was found for temperatures $0.166158 < T < 0.166162$. The magnetization is measured on each site. All three spin waves are plotted.

6 Summary

The *DMRG* method has been used to investigate incommensurate structures in 2D classical model for the first time. We found that it reproduces well the previous results for the ANNNI model. In the case of the ATNNI model it has shown much better performance in the regions where the previous approaches (the cluster transfer matrix method [24, 25] near $H = 2.4$ and the free-fermion approximation [12] for $H > 3$) has failed.

In [12] on the basis of scaling properties of Monte Carlo calculations and the exact diagonalization of finite strips, the authors concluded that at $H \cong 3$ the IC structure disappears and at higher fields H the direct phase transition between commensurate $\langle II \rangle$ and disordered phases is continuous.

We have observed the IC phase everywhere between the disordered and commensurate $\langle II \rangle$ phases, i.e. we have found no Lifshitz point where the three phases meet: commensurate, incommensurate, and disordered. Nevertheless, measured widths of the IC phase are extremely small at large H and exponentially tend to zero at $H = 4.8$. As the width of the IC phase gets narrower for the high-order approximations we cannot completely exclude the scenario of Domany and Schaub [12].

Our belief in correct description of incommensurate phases by the *DMRG* technique is supported by the reproduction of the ANNNI phase diagram with generally expected features.

Acknowledgments

This work has been supported by Slovak Grant Agency, Grant n. 2/4109/98. We would like to thank the organizers of the DMRG Seminar and Workshop in Dresden for the opportunity to participate in the meetings, especially for the useful discussion with T. Nishino and I. Peschel. A. G. also thanks P. Markoš for useful discussions and comments.

References

- [1] S. R. White, Phys. Rev. Lett. **69**, 2863 (1992); Phys. Rev. B **48** 10345 (1993).
- [2] T. Nishino, J. Phys. Soc. Jpn. **64**, 3598 (1995).
- [3] S. Östlund and S. Rommer, Phys. Rev. Lett. **75**, 3537 (1995); Phys. Rev. B **55**, 2164 (1997); K. Okunishi, Y. Hieida and Y. Akutsu, cond-mat/9810239.
- [4] P. Pajerský and A. Šurda, J. Phys. A: Math. Gen. **30** 4187 (1997).
- [5] A. Šurda, Acta Phys. Slov. **49**, 325 (1999).
- [6] K. Hallberg, cond-mat/9910082.
- [7] E. Carlon and A. Drzewiński, Phys. Rev. Lett. **79**, 1591 (1997).
- [8] T. Nishino and K. Okunishi, J. Phys. Soc. Jpn. **64** 4084 (1995).
- [9] R. Baxter, J. Math. Phys. **9**, 650 (1968); J. Stat. Phys. **19**, 461 (1978).
- [10] T. Nishino and K. Okunishi, J. Phys. Soc. Jpn. **65** 891 (1996); Phys. Soc. Jpn. **66** 3040 (1997); T. Nishino, K. Okunishi and M. Kikuchi, Phys. Lett. A **213**, 69 (1996).
- [11] T. Nishino and K. Okunishi, J. Phys. Soc. Jpn. **67**, 3066 (1998).
- [12] E. Domany and B. Schaub, Phys. Rev. B **29** 4095 (1983).
- [13] J. Villain and P. Bak, J. Phys. **42**, 657 (1981).
- [14] V. L. Pokrovsky and A. L. Talapov, Phys. Rev. Lett. **42**, 65 (1979).

- [15] H. J. Schultz, Phys. Rev. B **22**, 5274 (1980).
- [16] M. N. Barber and P. M. Duxbury, J. Phys. A **14**, L251 (1981).
- [17] M. E. Fischer and W. Selke, Phys. Rev. Lett. **44**, 1502 (1980).
- [18] F. D. M. Haldane, P. Bak, and T. Bohr, Phys. Rev. B **28**, 2743 (1983).
- [19] A. Gendiar and A. Šurda in preparation.
- [20] E. Carlon, M. Henkel, and U. Schollwöck, Europhys. J. B to appear (1999).
- [21] P. Nightingale, J. Appl. Phys. **53**, 7927 (1982).
- [22] R. J. Baxter, Exactly Solved Models in Statistical Physics, Academic Press, London (1982).
- [23] W. Selke, Phys. Rep. **170**, 213 (1988); W. Selke, *Phase Transition and Critical Phenomena* vol. **15** (New York: Academic) (1992).
- [24] I. Karasová and A. Šurda, J. Stat. Phys. **70**, 675 (1993).
- [25] L. Tóth and A. Šurda (unpublished).